An Integrated Power Module Based on the Power-System-In-Inductor Structure

Laili Wang, *Senior Member, IEEE*, Wenbo Liu, *Student Member, IEEE*, Doug Malcom, and Yan-Fei Liu, *Fellow, IEEE*

***Abstract*—This paper presents an integrated power module with the features of high power density and high efficiency. A multifunctional integrated magnetic component is designed. The component has the roles of both the filter inductor and the package of the converter. With the assist of finite-element analysis, the design and optimization of the proposed inductor are demonstrated. It has higher inductance value than the inductor used in conventional designs. The package is composed of bigger copper winding and higher thermal conductive magnetic material, leading to lower direct current resistance and better thermal performances than conventional transfer molding packaging. Benefiting from these advantages, the power module built based on the inductor can achieve higher efficiency and lower temperature rise than those based on traditional plastic packaging solution. Design of the inductor is demonstrated through the combination of analytical and simulation methods. An inductor prototype is built and used in an integrated power module to do experimental tests. Loss breakdown of the module is analyzed. The performances of the proposed power module are better than the conventional transfer molding packaging solution with the same board or other state-of-art products.**

***Index Terms*—Inductor design, magnetic integration, power density, power-system-in-inductor (PSI^2), thermal performance.**

I. Introduction

POWER modules have been widely used in telecom equipment, computer servers, and consumer electronics to provide solutions of power management. In a small package, the power modules should integrate all the functions of dc/dc converters based on the solution of discrete so that the system design engineers do not need to spend too much time on the power supply solution, thereby saving time for products development. Besides, an integrated power module has better performance than the solution of discrete components in terms of reliability and space saving.

Manuscript received June 15, 2017; accepted October 17, 2017. Date of publication December 7, 2017; date of current version June 22, 2018. This work was supported by the Young Scientists Fund of the National Natural Science Foundation of China under Grant 51607141. This paper was presented in part at the IEEE Applied Power Electronics Conference and Exposition, Long Beach, CA, USA, Mar. 2016. Recommended for publication by Associate Editor C. Fernandez. *(Corresponding author: Laili Wang.)*

L. Wang is with the State Key Laboratory of Electrical Insulation and Power Equipment, Xi'an Jiaotong University, Xi'an 710049, China (e-mail: llwang@mail.xjtu.edu.cn).

W. Liu and Y.-F. Liu are with Queen's University, Kingston, ON K7L3N6, Canada (e-mail: liu.wenbo@queensu.ca; yanfei.liu@queensu.ca).

D. Malcolm is with Sumida Technologies Inc., Kingston, ON K7L 4V1, Canada (e-mail: doug_malcolm@us.sumida.com).

Color versions of one or more of the figures in this paper are available online at http://ieeexplore.ieee.org.

Digital Object Identifier 10.1109/TPEL.2017.2769681

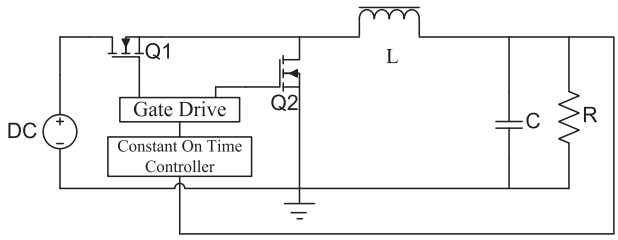

Fig. 1. Schematic and picture of a step-down power module.

Nonisolated step-down power modules are the most popular power modules used in today's industry. They are composed of an integrated buck regulator (or controller with two MOSFETs), an inductor, some input and output capacitors, and some auxiliary components. Fig. 1 shows the schematic of the buck converter in a step-down power module. There are quite a few literature discussing about the design of power modules through increasing switching frequency [1]–[5], using topologies without magnetics [6]–[9], and package and integration technology [10]–[36]. Embedding magnetics and capacitors in the printed circuit boards (PCBs) is demonstrated in [22]; however, core loss of the embedded magnetic material is significant. Low temperature cofired ceramic technology becomes very popular in research works and can achieve very high power density [23]–[25], [29]–[36]. Microinductor and microtransformer based on thin film technology is another key technology used for power modules [26]–[28]. The disadvantage of this technology is that it has higher direct current resistance (DCR) which causes more loss than conventional inductors.

In industry, there are two typical packaging solutions for making the power modules. One is based on PCB substrate. The semiconductor die, metal powder composite inductor, and other parts are soldered or wire bonded on the substrate, and the whole substrate is packaged using injection molding. The other one is based on lead frame. In this way, all the components are connected to the lead frame through wire-bonding, and the whole module is then packaged with injection molding. No matter which technology is employed to package the module, the inductor is a necessary part in a buck converter. And to leave some space for plastic material, the inductor should be smaller than the package size. It generally takes up about 1/4–1/3 of the whole volume of the module.

This paper proposes a new packaging technology called power-system-in-inductor (PSI^2). A customized magnetic component is designed, acting as both the package of the whole

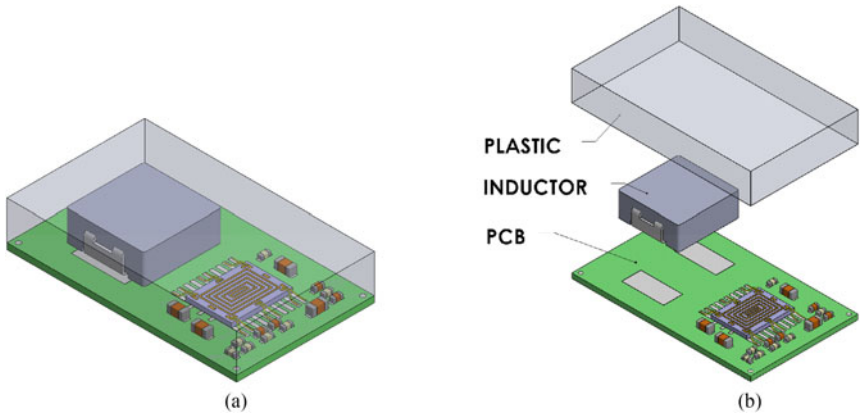

Fig. 2. Conventionl plastic packing. (a) Transfor molding power module. (b) Internal structure.

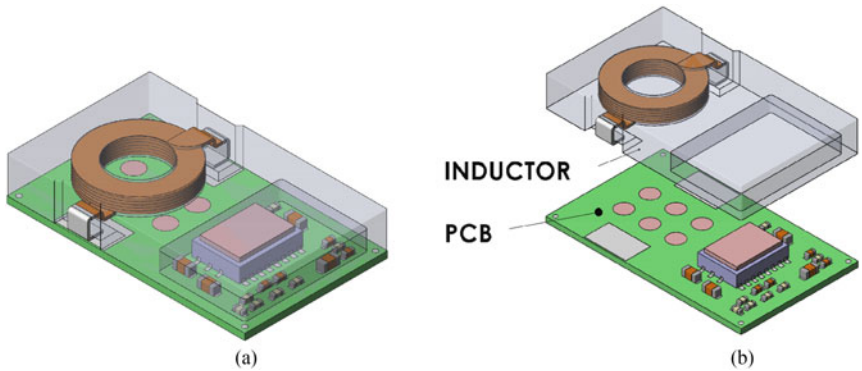

Fig. 3. Proposed magnetic packaging. (a) Magnetic packaing power module. (b) Internal structure.

power module and the filter inductor of the converter. Section II of this paper presents the structure of the power module; Section III presents the design of the customized inductor based on the combination of analytical and simulation methods. Section IV will build a prototype and do comparison experiments with plastic packaging solution and other state-of-art products. Section V concludes this paper.

II. Principle of Structure

This section will first introduce the disadvantage of the traditional transfer molding packaging, and then describe the newly proposed magnetic packaged power module with the purpose of having better electrical and thermal performance. Structural comparison between the two kinds of package will be illustrated in detail.

Commercial power modules in the market are generally packaged with plastic material by the injection molding process. It has a regulator (can be a controller and two discrete MOSFETs in the multiple chips version), an inductor, and some auxiliary components mounted on the substrate together, and then the whole substrate is packaged with plastic material. Fig. 2 shows the structure of the traditional transfer molding packaged power module. It follows the standard IC packaging process; however, there are several disadvantages for power modules. First, in transfer molding packaging, a small inductor which is certainly smaller than the plastic packaging is used; it will have fairly higher DCR or lower inductance than an inductor of bigger size. Second, plastic material is used to package the heat sources (internal IC and inductor), which inevitably increases the thermal resistance from the heat sources to ambient. Third, the packaging process will add extra cost on the power module.

To solve aforementioned issues, a new magnetic packing power module is proposed. Fig. 3 shows the structure of the proposed power module. The proposed structure has a regulator, some auxiliary components, and an inductor mounted on the PCB. In contrast to conventional plastic packaged power modules, the magnetic package has both the roles of encapsulation and the inductor of the converter. The magnetic core has a cavity in one half and an embedded coil in the other half. The buck regulator and the auxiliary components are embedded underneath the cavity. Thermally conductive glue is used to attach the top of the regulator to the ceiling of the cavity with the purpose of transferring heat from the regulator to the magnetic core. The embedded coil forms an inductor together with the magnetic core. Therefore, the magnetic core has functions of both power module package and filter inductor in the converter. Benefiting from this package technology, the proposed converter has two advantages over the power modules based on conventional transfer molding package technology. First, without the necessity of leaving enough room for plastic packaging, the inductor size could be as big as the package size, which

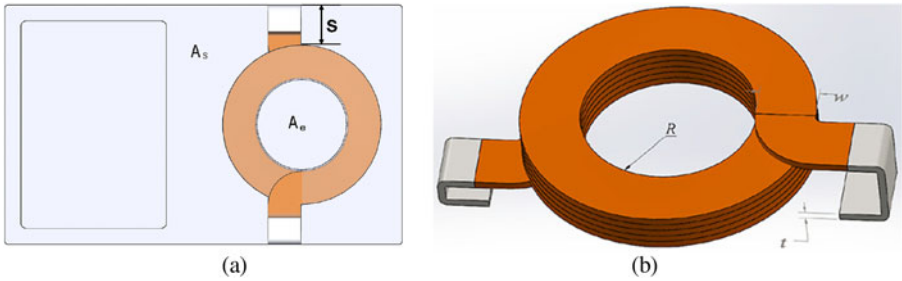

Fig. 4. Dimension of the winding.

means that both the winding and magnetic core will be bigger than those of the inductors used in plastic packing. Compared with a conventional plastic packaged power module with a small metal powder composite inductor inside, the proposed magnetic packaged power module has lower DCR and higher inductance value since the volume of the inductor is larger. Second, in the power module, the heat sources are the semiconductor devices and the inductor. The inductor, composed of magnetic material which has higher thermal conductivity than plastic, is directly exposed to the ambient. There is no other material on the top of inductors increasing the thermal resistance from the hot sources to the ambient. It means that the magnetic package power module has lower temperature, which will in turn improve the other performances of the whole power module. Third, no injection molding process is required for magnetic packaged power module, which will be beneficial to reduce the total cost.

III. Inductor Design and Analysis

This section will present the design of the proposed inductor for a 12-V input, 5-V/8-A output, 15 mm × 9 mm × 2.8 mm power module. According to the design specification of the power module, the required inductance value is 1 μH. Benefiting from the proposed structure, the inductor has the same width as the module itself. Therefore, the whole magnetic core is 15 mm × 9 mm × 2.4 mm (the substrate is 0.4 mm), and the effective volume for putting the winding in is 9 mm × 9 mm × 2.4 mm. For this given inductance and volume, the winding should be designed to haves the smallest DCR.

There are quite a few papers [29]–[40] discussing the model of inductance calculation and design. Most of them are for inductors on the semiconductor or PCB, which are not suitable for inductor design in this paper. Since the magnetic core has a customized shape, and there is no existing models for calculating the inductance, analytical calculation is first employed to obtain the possible number of turns, then finite-element analysis (FEA) is used to analyze the relationship between the inductance *L*, coil radius *R*, coil width *w*, and wire thickness *t* based on 9 mm × 9 mm × 2.4 mm size (effective volume for winding) with the purpose of further optimizing the parameters.

Analytical model is first derived to calculate the number of turns for winding which is made of planar copper wire. Fig. 4 shows the top view of the winding and its dimension parameters. A_s and A_e are the areas of magnetic material through which the flux goes through. During the analytical calculation, they are assumed to be equal to each other so that the design process of the magnetic path is simplified when calculating the number of turns. The inductance calculating equation is expressed in

$$L = \frac{\mu_r \mu_0 N^2 A_e}{l} \tag{1}$$

where A_e is the effective area for flux density, *l* is the length of magnetic path, *N* is the number of turns, and μ_r is the relative permeability of the magnetic material. Both A_e and *l* highly depend on the radius *R*, width *w*, and thickness *t* of the coil. The effective area A_e can be calculated by

$$A_e = \pi \cdot r^2. \tag{2}$$

The estimated magnetic path length can be calculated through

$$l = 2h + 2w + r \tag{3}$$

where *h* is the total thickness of the winding, and it can be expressed by the height of the inductor *H* and thickness of magnetic material above or below the winding *e* in

$$h = H - 2e. \tag{4}$$

Substituting (2)–(4) into (1) yields

$$N = \sqrt{\frac{L(2(H-2e)+2w+r)}{2\mu_r \mu_0 \pi r^2}}. \tag{5}$$

The flux density can be calculated by (6) to assure that the magnetic material will not become saturated at full load. However, more accurate flux density distribution can be obtained by simulation to validate the design since the magnetic path is not in regular shape

$$B = \frac{LI}{NA_e}. \tag{6}$$

In this design, the total height of the inductor *H* is 2.4 mm. Thickness of magnetic materials above and below the winding *e* is set to be 0.65 mm; the relative permeability of the magnetic material μ_r is 10 and the proposed inductance value is 1 μH. Number of turns is calculated by substituting these parameters into (5) and sweeping internal radius *r* and conductor width *w*. Table I shows the calculated results. The number of turns increases with the decrease of the internal radius *r* and increases with the width of the coil *w*. For the proposed inductor in this paper, the number of turns should include a half turn since it has two terminals leading out from two sides. Therefore, the calculated number of turns should be modified to number of

TABLE I
CALCULATED NUMBER OF TURNS FOR THE PROPOSED INDUCTOR

r (mm) \ w (mm)	1.00	1.20	1.40	1.60	1.80	2.00	2.20	2.40	2.60	2.80	3.00
1.0	8.1	8.4	8.7	9.0	9.3	9.6	9.8	10.1	10.3	10.6	10.8
1.25	6.6	6.9	7.1	7.3	7.6	7.8	8.0	8.2	8.4	8.6	8.8
1.50	5.7	5.9	6.1	6.2	6.4	6.6	6.8	6.9	7.1	7.2	7.4
1.75	5.0	5.1	5.3	5.4	5.6	5.7	5.9	6.0	6.2	6.3	6.4
2.00	4.4	4.6	4.7	4.8	5.0	5.1	5.2	5.3	5.5	5.6	5.7
2.25	4.0	4.1	4.3	4.4	4.5	4.6	4.7	4.8	4.9	5.0	5.1
2.50	3.7	3.8	3.9	4.0	4.1	4.2	4.3	4.4	4.5	4.6	4.7
2.75	3.4	3.5	3.6	3.7	3.8	3.9	4.0	4.0	4.1	4.2	4.3
3.00	3.2	3.3	3.4	3.4	3.5	3.6	3.7	3.8	3.8	3.9	4.0

TABLE II
PRACTICAL DESIGN NUMBER OF TURNS FOR THE PROPOSED INDUCTOR

r (mm) \ w (mm)	1.00	1.20	1.40	1.60	1.80	2.00	2.20	2.40	2.60	2.80	3.00
1.0	8.5	8.5	8.5	9.5	9.5	9.5	9.5	10.5	10.5	10.5	10.5
1.25	6.5	6.5	7.5	7.5	7.5	7.5	8.5	8.5	8.5	8.5	8.5
1.50	5.5	5.5	6.5	6.5	6.5	6.5	6.5	6.5	7.5	7.5	7.5
1.75	5.5	5.5	5.5	5.5	5.5	5.5	5.5	6.5	6.5	6.5	6.5
2.00	4.5	4.5	4.5	4.5	5.5	5.5	5.5	5.5	5.5	5.5	5.5
2.25	4.5	4.5	4.5	4.5	4.5	4.5	4.5	4.5	4.5	5.5	5.5
2.50	3.5	3.5	3.5	4.5	4.5	4.5	4.5	4.5	4.5	4.5	4.5
2.75	3.5	3.5	3.5	3.5	3.5	3.5	4.5	4.5	4.5	4.5	4.5
3.00	3.5	3.5	3.5	3.5	3.5	3.5	3.5	3.5	3.5	3.5	4.5

turns in a practical design as shown in Table II. Inductance value calculated based on the Table II is still close to 1 μH although there should be some variations. Based on the calculation and modification, the number of turns can be 3.5, 4.5, 5.5, 6.5, 7.5, 8.5, 9.5, and 10.5 depending on the radius and coil width. Even with a simulation tool, it is still very time-consuming to simulate every case of turns. Some of the cases can be easily excluded because of their higher DCR. The equation of DCR calculation is shown in

$$R_{\mathrm{DC}} = \rho \frac{2\pi N \cdot \left(r + \frac{w}{2}\right)}{\left(\frac{H - 2e}{[N]} - u\right) \cdot w} \tag{7}$$

where N is the number of turns listed in Table II, ρ is the resistivity of the copper, u is the thickness of the insulation

TABLE III
CALCULATED DCR

w (mm) / *r* (mm)	**1.00**	**1.20**	**1.40**	**1.60**	**1.80**	**2.00**	**2.20**	**2.40**	**2.60**	**2.80**	**3.00**
1.0	46.3	41.1	37.5	72.3	67.8	64.2	61.3	215.8	208.2	201.8	196.2
1.25	17.5	15.5	23.9	22.0	20.5	19.3	33.0	31.5	30.3	29.2	28.3
1.50	11.7	10.3	15.8	14.4	13.4	12.5	11.8	11.3	18.5	17.8	17.2
1.75	13.2	11.5	10.3	9.4	8.6	8.1	7.6	12.3	11.8	11.3	10.9
2.00	8.3	7.2	6.4	5.8	9.5	8.8	8.3	7.8	7.5	7.1	6.9
2.25	9.1	7.9	7.0	6.3	5.8	5.4	5.1	4.8	4.5	7.7	7.3
2.50	5.2	4.5	4.0	6.9	6.3	5.8	5.4	5.1	4.9	4.6	4.4
2.75	5.7	4.9	4.3	3.9	3.5	3.3	5.8	5.5	5.2	4.9	4.7
3.00	6.1	5.2	4.6	4.1	3.8	3.5	3.2	3.1	2.9	2.7	5.0

layer, and [*N*] is the ceiling integral of the calculated number of turns listed in Table I.

Table III lists the calculated DCR values obtained through (7). The DCR value increases with the reduction of internal radius *r* and the increase of the number of turns *N*. When $r =$ 1.0, 1.5 mm, the DCR are much higher than other cases, so they are excluded from the candidates. The left solutions have the number of turns 3.5, 4.5, 5.5, and 6.5. Those four winding solutions will be put into simulation to do further analysis.

The number of turns is obtained through (5) by assuming that the total inductance value is 1 μH. However, it is only used to calculate the rough number of turns. The inductor designed with the parameters in the calculation might not get the exact inductance. This is because (5), which uses the calculated inductance of closed magnetic path with constrained regular effective area A_{e} such as *E I* ferrite magnetic cores, can introduce some error in inductance calculation. The proposed inductor does not have constant effective area A_{e} along the magnetic path. The equivalent length of the magnetic path could also contribute some error. An FEA simulation for each number of turns is executed to further get the right parameters for the inductor. Figs. 5 and 6 show the simulated inductance and DCR for different number of turns. For all the cases, the inductance value has the trend of increase with the increase of radius *r* while it has the trend of decrease with the increase of the coil width *w*. The maximum radius varies for different values of coil width since the outer diameter expressed in (8) is limited by the width of the magnetic core 9 mm which means $r + w$ should be less than 4.5 mm in the simulation. DCR of the inductor has the same trend as the inductance. It increases with the increase of radius *r* and reduces with the increase of coil width *w*. Therefore, the design of such an inductor is essentially choosing the right parameters to reduce DCR while achieving the expected inductance value. For the 3.5 turn design, DCR is very small since it has less number of turns and thicker copper for each turn, but the inductance value is not high enough to meet the requirement of 1 μH specification. It can be excluded from the comparison, then only 4.5 turn, 5.5 turn, and 6.5 turn are further considered as candidates. For the 4.5 turn design, the maximum inductance value can be higher than 1 μH, and it is at about $r = 2.75$ mm, $w = 1$ mm. There are some points, which are not shown in the curves, reaching 1 μH point. For example, $r = 2.85$, $w = 1.1$ mm, they are very similar to the point $r = 2.75$ mm, $w = 1$ mm. For 5.5 turn design, there are three combinations. $r = 1.8$ mm, $w = 1$ mm; $r = 2$ mm, $w = 1.4$ mm; $r = 2.25$, $w = 1.8$. For 6.5 turn design, there are five candidates. $r = 1.2$ mm, $w =$ 1 mm; $r = 1.3$ mm, $w = 1.4$ mm; $r = 1.4$ mm, $w = 1.8$ mm; $r = 1.45$ mm, $w = 2.2$ mm; $r = 1.5$ mm, $w = 2.6$ mm. For different groups of parameters, the DCR shown in Fig. 6 is different

$$d = 2(w + r). \tag{8}$$

It is hard to determine through either the inductance value curves or the DCR value curves because the design of an inductor is essentially finding the tradeoff point of the inductance and DCR under the specified volume 9 mm $\times$ 9 mm $\times$ 2.4 mm and inductance 1 μH. A new parameter *L/R* is defined in this paper as a new criterion to choose and optimize the design. It should

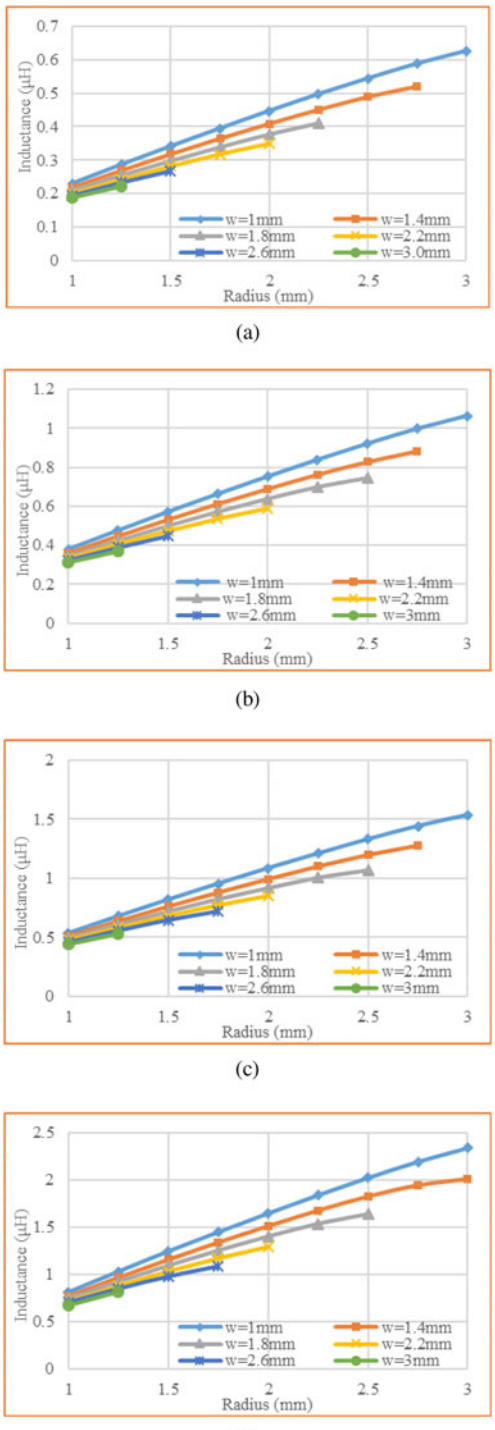

Fig. 5. Inductance versus radius with coil width as a parameter. (a) $N = 3.5$. (b) $N = 4.5$. (c) $N = 5.5$. (d) $N = 6.5$.

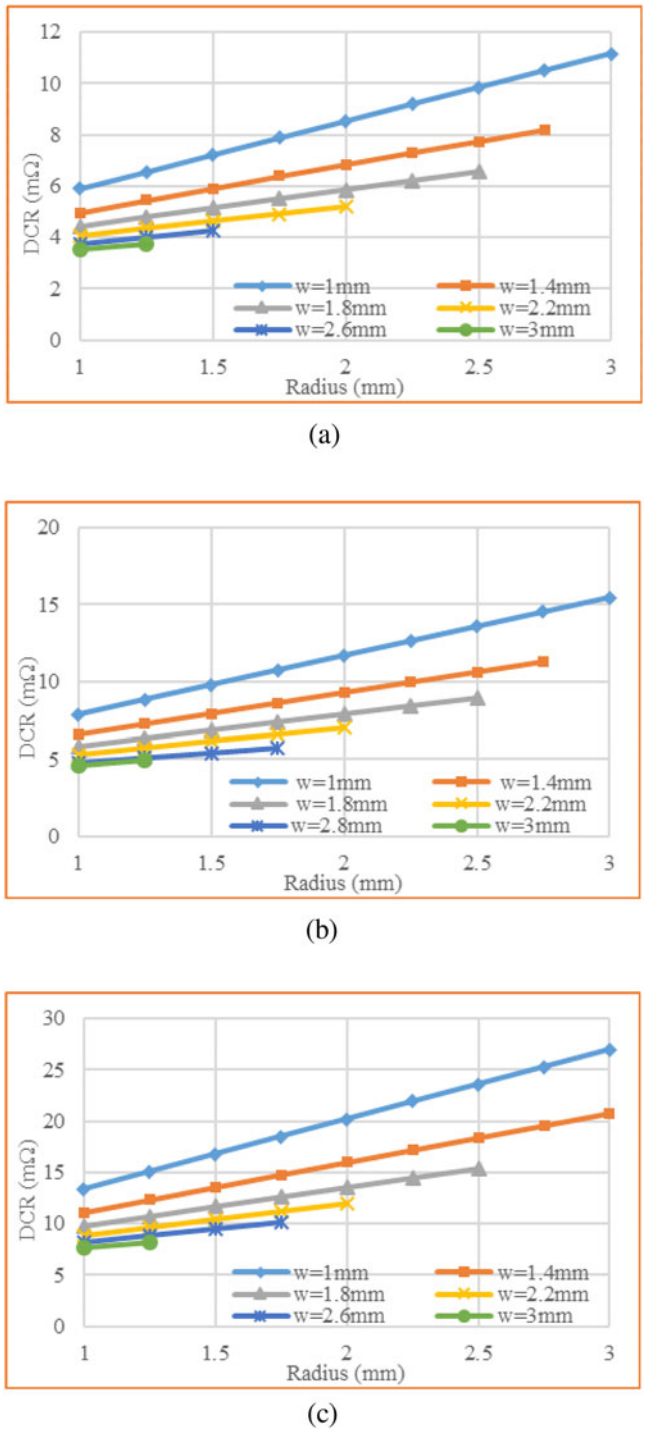

Fig. 6. DCR versus radius with coil width as a parameter. (a) $N = 4.5$. (b) $N = 5.5$. (c) $N = 6.5$.

be noted that this parameter is different from the quality factor $\omega L/R$ which also reflects the ac performance of the magnetics. It is manly used to show the low-frequency characteristics of an inductor. Fig. 7 shows the curves of L/R for number of turns 4.5, 5.5, and 6.5. It can be observed that the L/R is higher for $N = 5.5$ than the other two number of turns for the same radius and coil and L/R of the selected candidates.

In Table IV, No. 4 ($N = 5.5, r = 2.25$ mm, $w = 1.8$ mm) has the lowest DCR and the highest L/R. However, the $r + w$ value is 4.05 which is close to half-width of the module. In the real practice of manufacture, by considering the mechanical stress of the magnetic material when bending the coil terminals, there should be 3 mm margin (1.5 mm on both sides), which means $r + w \leq 3$ mm. With this restriction applied to the candidates, three options are left. They are No. 2 ($N = 5.5$, $r = 1.8$ mm,

TABLE IV
SIMULATION RESULTS OF THE SELECTED CANDIDATES

No.	1	2	3	4	5	6	7	8	9
Turns	4.5	5.5	5.5	5.5	6.5	6.5	6.5	6.5	6.5
Radius (mm)	2.75	1.8	2	2.25	1.2	1.3	1.4	1.45	1.5
Width (mm)	1	1	1.4	1.8	1	1.4	1.8	2.2	2.6
$r + w$ (mm)	3.75	2.8	3.4	4.05	2.2	2.7	3.2	3.65	4.1
DCR (mΩ)	10.5	10.8	9.28	8.4	15	12.5	11.3	9.52	9.5
L/DCR (μH/mΩ)	0.095	0.088	0.107	0.12	0.068	0.080	0.093	0.098	0.103

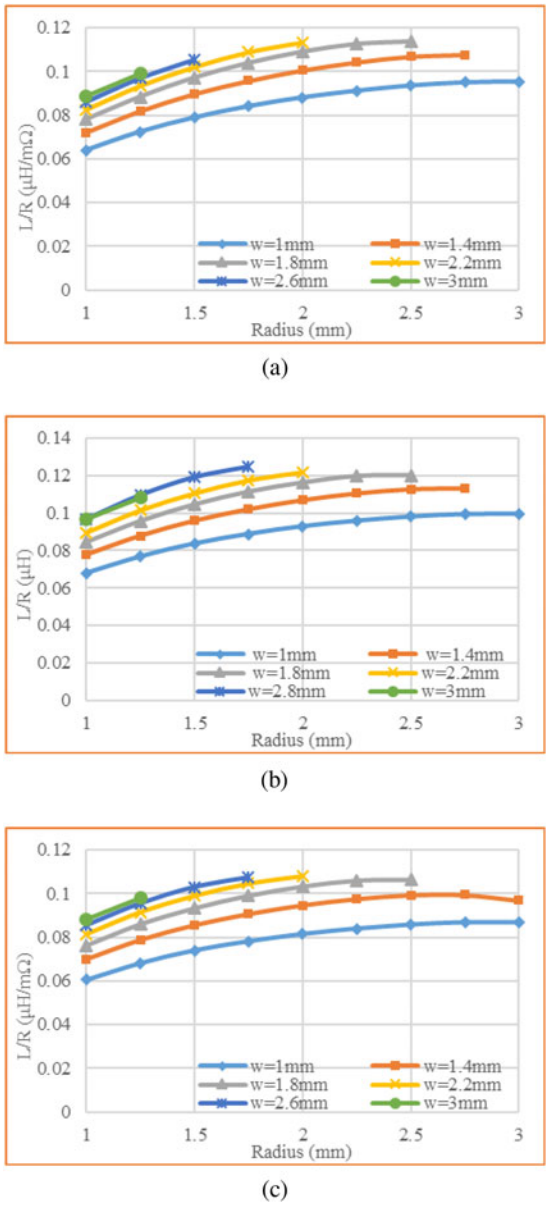

Fig. 7. L/R versus radius with coil width as a parameter. (a) $N = 4.5$. (b) $N = 5.5$. (c) $N = 6.5$.

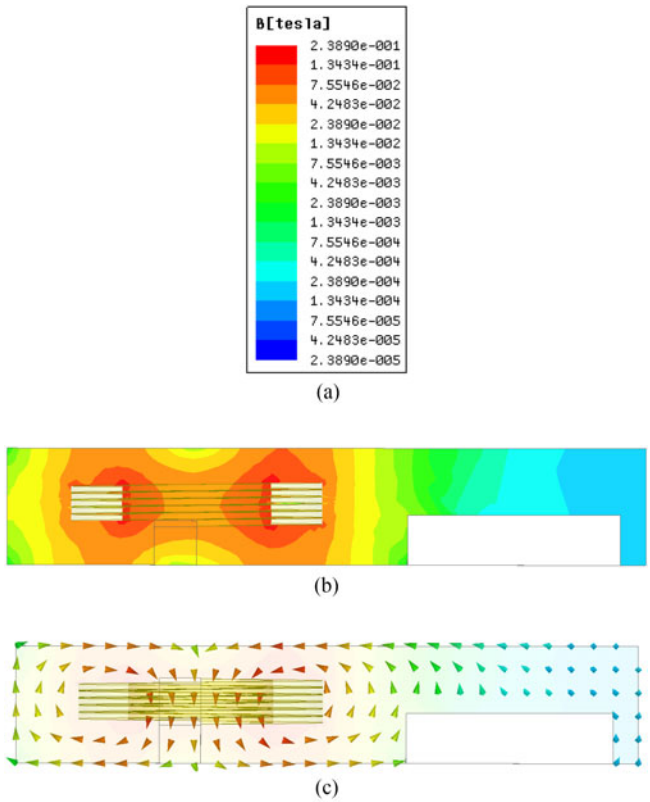

Fig. 8. Simulated flux distribution. (a) Scalar. (b) Magnitude flux density. (c) Vector flux density.

$w = 1$ mm), No. 5 ($N = 6.5, r = 1.2$ mm, $w = 1$ mm) and No. 6 ($N = 6.5$, $r = 1.3$ mm, $w = 1.4$ mm). No. 2 has the highest L/R value and it can be selected as a final design. Since the $r + w$ value for No. 2 is 2.8 mm, w can be further increased by 0.2 mm ($r + w$ is not larger than 3 mm) which will not lead to significant decrease of the inductance value. And prototypes will be made based on this parameters ($N = 5.5$, $r = 1.8$ mm, $w = 1.2$ mm). A new simulation is executed based on the selected parameters. The inductance value at no load is 1.1 μH; it drops to 1.01 μH at full load. A field distribution of flux density at 6-A current excitation in the designed inductor is shown in Fig. 8. The maximum flux density happens around the winding, which is 0.24 mT. The saturation flux density of the magnetic materials is about 1 T. Therefore, the inductor still has the potential to be used in higher output current application, such as 12-V input, 5-V/8-A output power module.

IV. PROTOTYPE AND EXPERIMENT

In this section, inductor prototype is made to assemble an integrated power module which is used to do tests and loss

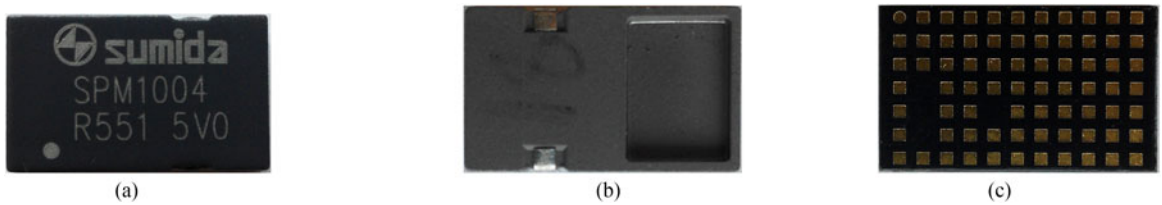

Fig. 9. Picture of the power module. (a) Top view. (b) Bottom view of the inductor. (c) Bottom view of the module.

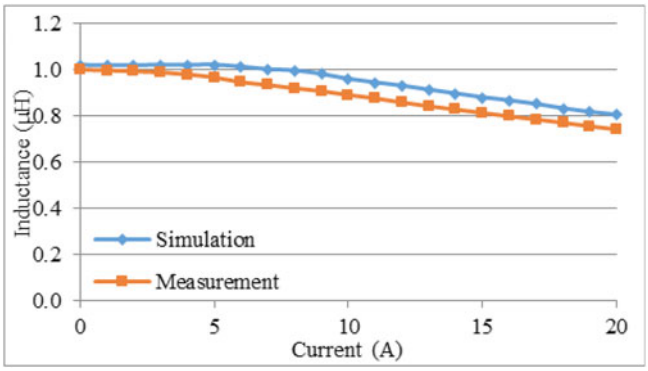

Fig. 10. Inductance value of the proposed inductor versus dc bias.

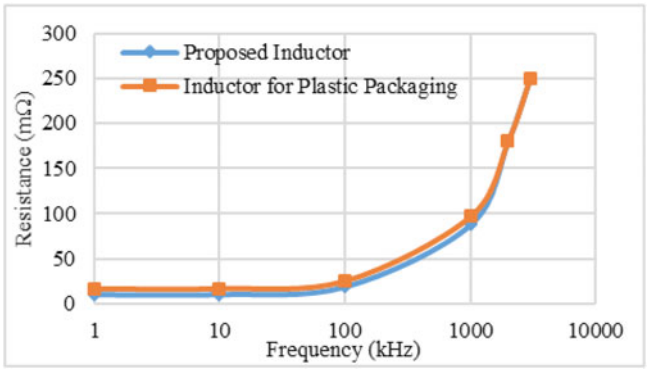

Fig. 11. Resistance versus frequency.

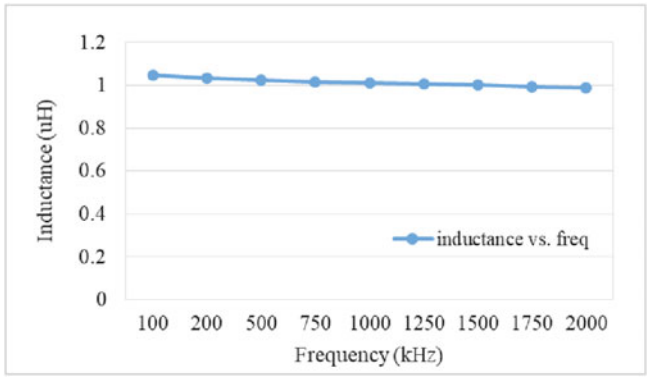

Fig. 12. Inductance versus frequency.

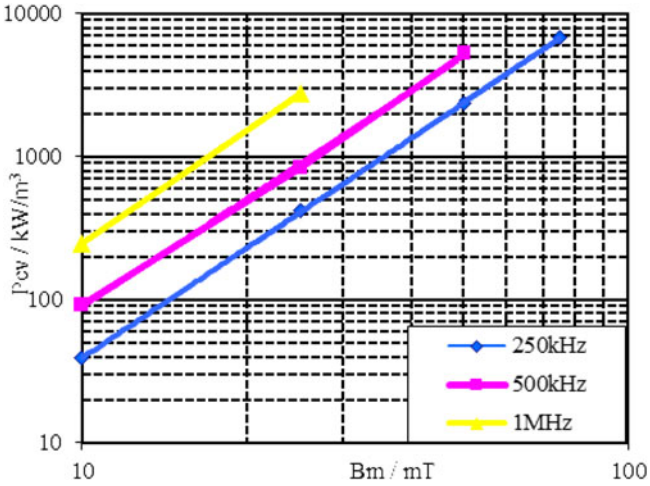

Fig. 13. Loss characteristics of the magnetic material.

analysis. Fig. 9(a) and (b) shows the top view and bottom view of the inductor. Two leads were extended from the winding and bended at the bottom of the inductor for soldering on the small PCB which is 0.4 mm thick. Discrete components, such as regulator and resistors in the power circuit, are soldered on the area of PCB under the cavity of the inductor. Red glue is used at the bottom of the magnetic core where winding is embedded and the ceiling of the cavity where the regulator chip is located to strengthen the adhesive force during the assembling process. Fig. 9(c) shows the bottom view of the assembled power module. Before assembling the inductor on the PCB, inductance versus dc bias is measured using a Wayne Kerr 3260B *LCR* meter. With the purpose of comparison, it is also simulated through FEA simulation. Fig. 10 shows the test and simulation results. They correlate with each other very well. Fig. 11 shows the resistance versus switching frequency by measurement and simulation. Fig. 12 shows the measure inductance versus switching frequency. The power module is then soldered on an evaluation board to do loss analysis and tests of performance. Loss characteristics of the magnetic material are first tested to obtain the parameters of Stenmez equations in FEA simulation to calculate the core loss.

Fig. 13 shows the power loss of the magnetic materials versus flux density with frequency as a parameter. With the simulated core loss, loss breakdown of the power module is executed. Fig. 14 shows the loss of the inductor and the switches.

Two experiments of comparison are accomplished with the assembled power module to verify its performance. The first one is to show the advantage of the proposed packaging technology over the conventional plastic packing technology by using the same PCB and circuit but different inductors and packaging. The second one is to compare the performances of the proposed power module with the state-of-art plastic packaging power modules in industry.

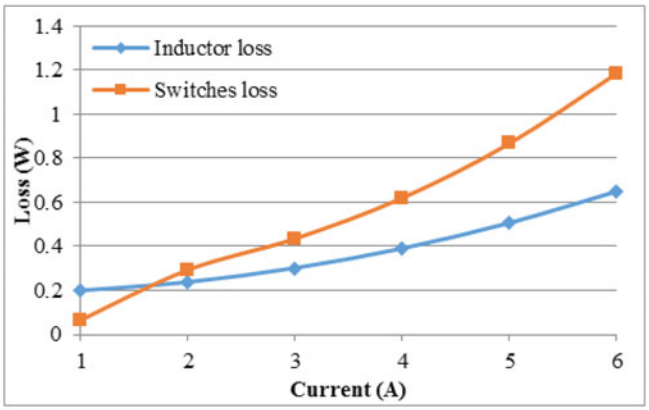

(a)

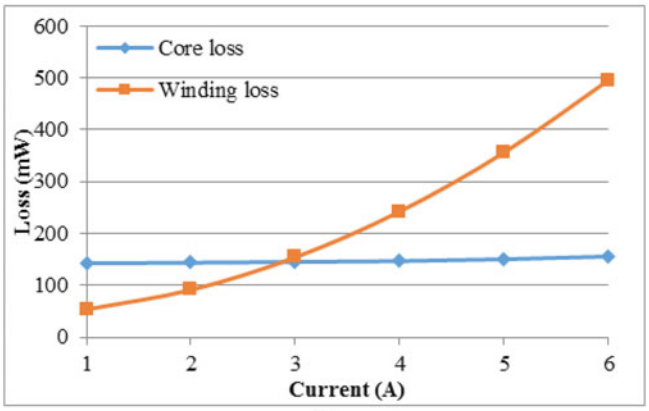

(b)

Fig. 14. Loss breakdown of the power module. (a) Loss of the inductor and switches. (b) Loss of the winding and magnetic core.

Fig. 15. Picture of the selected metal powder composite inductor for plastic packaging.

A. *Experimental Comparison of the Power Module With Different Inductors and Packaging*

As described in Section I, one of the advantages of the proposed power module is that it is able to have inductor with larger volume than that in conventional plastic packaging which has to leave enough room for injecting plastic material during packaging process. For inductors made with the same magnetic material, larger volume means higher inductance value and lower DCR. Fig. 15 shows the picture of the selected metal powder composite inductor used for plastic packaged module. The metal powder composite inductor designed for the plastic packaging has to be smaller than the module to leave enough room for plastic packaging. Generally, the thickness of the plastic layer is around 1 mm thick for power modules. By considering the extended soldering points (0.5 mm) on the inductor leads, the volume of the inductor is selected to be 6 mm $\times$ 6 mm $\times$ 2.2 mm. It has 0.9-μH inductance value and 17-mΩ DCR. Fig. 16 shows its inductance value versus dc bias. The prototype of the proposed inductor has 1-μH inductance value and 11-mΩ DCR. The inductor for plastic packaging has much smaller saturation current than the proposed inductor because it has smaller volume, thus smaller effective area to for the flux. Both inductors are soldered on the same PCB to test their efficiencies under the same conditions. Fig. 17 shows the small board with selected metal composite powder inductor soldered on it. Fig. 18 shows the efficiency comparison results. It can be observed that the

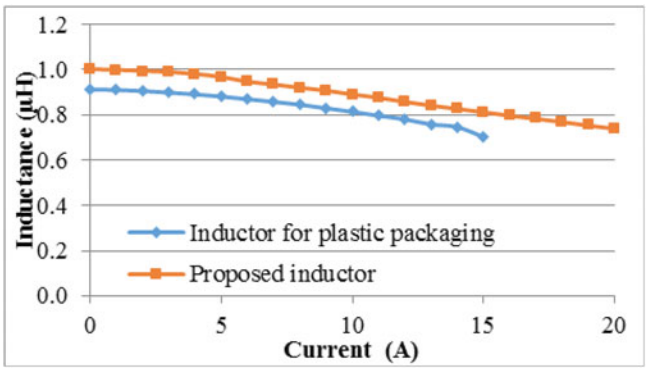

Fig. 16. Inductance of the proposed inductor and the selected inductor for plastic packaging.

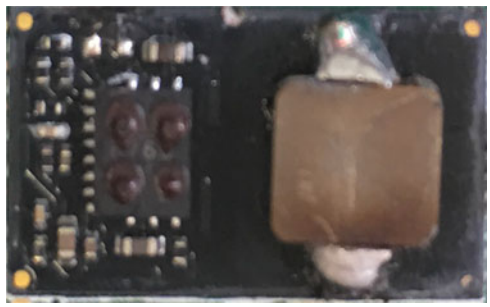

Fig. 17. PCB of the power module with the selected metal powder composite inductor.

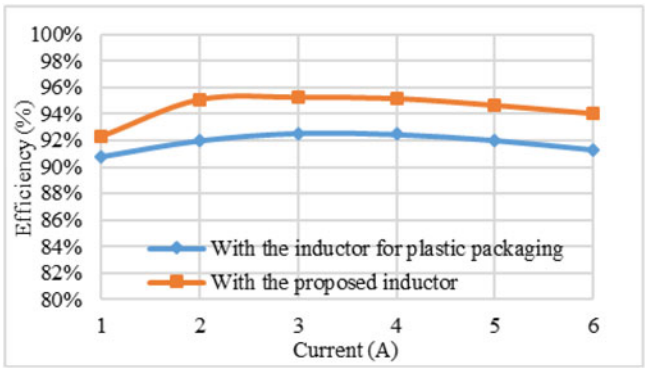

Fig. 18. Efficiency curves of the power modules with different inductors.

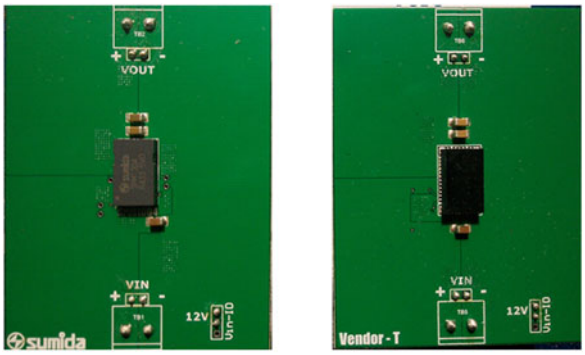

Fig. 19. Test boards with power modules. (a) Proposed power module. (b) Commercial product.

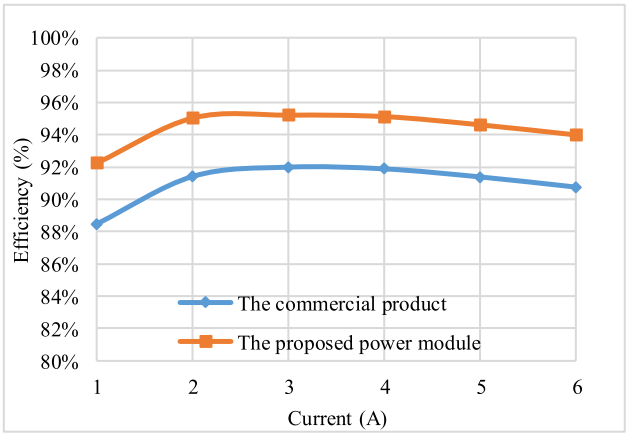

Fig. 20. Efficiency of the two power modules.

PCB with the proposed inductor has about 2% higher efficiency across the whole load range since it has lower DCR.

B. Experimental Comparison of the Power Module With State-of-Art Power Module

Besides comparison based on the same PCB and circuit, comparison between the proposed power module and a state-of-art commercial product which has different PCB and circuit is also presented in this part. A popular commercial product is selected. It is a 12-V normal input, 6-A output part with the same volume of the proposed power module, but the internal inductor is still not as big as the proposed inductor. Fig. 19 shows the pictures of both the proposed power module and the commercial product soldered on the same size evaluation board for testing their efficiencies and thermal performances. Both modules have 12-V input and 5-V output. The proposed power module has 780-kHz switching frequency while the commercial product has 800-kHz switching frequency. Fig. 20 and Fig. 21 shows the efficiencies of the two modules. Benefiting from the packaging technology, the proposed module has 2% higher efficiency than the commercial product. Fig. 22 shows the thermal pictures of both power modules at 12-V input, 5-V/6-A output. The proposed power module has 12.9 °C lower temperature than the commercial

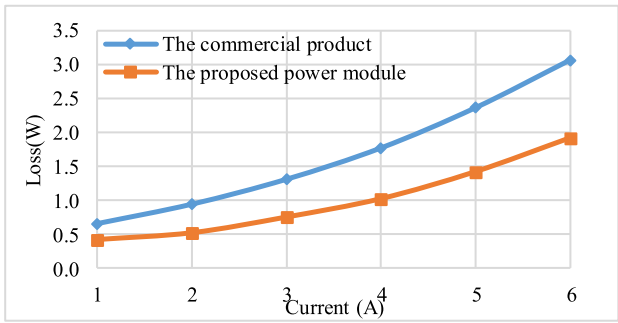

Fig. 21. Loss of the two power modules.

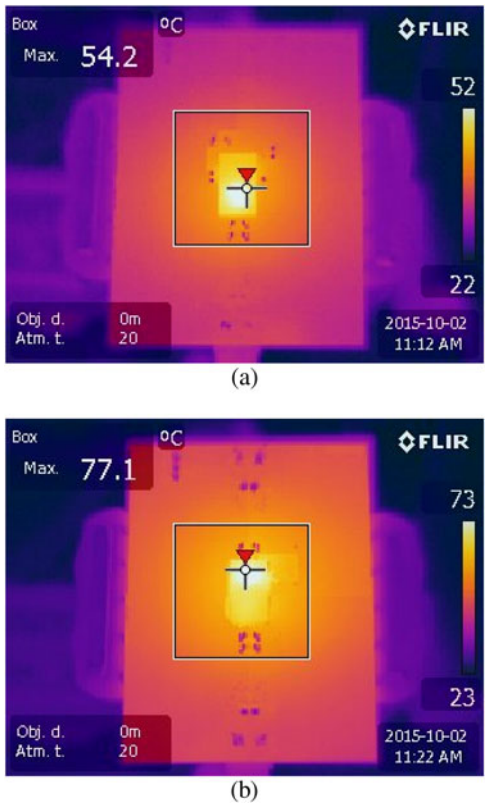

Fig. 22. Thermal images of the test boards with power modules at full load (5 V/6 A). (a) Proposed power module. (b) Commercial product.

product. There are two reasons for this phenomenon. First, the proposed power module has higher efficiency than the commercial product. The proposed power module has 1.9-W loss at full load while the commercial product has 3.1-W loss at full load; second, the proposed power module is packaged with magnetic material composed of iron powder, leading to smaller thermal resistance from the heat sources to the ambient than that of the commercial product.

V. Conclusion

The special magnetic component proposed in this paper integrates the functions of power inductor and packaging of the whole power module. A PSI^2 structured power module is designed based on the magnetic component to show its benefit

of system integration. Compared with conventional designs, the new design has higher inductance value and lower DCR. Experimental tests show that the designed power module has higher efficiency and better thermal performance than the state-of-art commercial power modules.

REFERENCES

[1] D. J. Perreault *et al.*, "Opportunities and challenges in very high frequency power conversion," in *Proc. 2009 24th Annu. IEEE Appl. Power Electron. Conf. Expo.*, Feb. 15–19, 2009, pp. 1–14.

[2] R. C. N. Pilawa-Podgurski, A. D. Sagneri, J. M. Rivas, D. I. Anderson, and D. J. Perreault, "Very-high-frequency resonant boost converters," *IEEE Trans. Power Electron.*, vol. 24, no. 6, pp. 1654–1665, Jun. 2009.

[3] A. D. Sagneri, D. I. Anderson, and D. J. Perreault, "Optimization of integrated transistors for very high frequency DC–DC converters," *IEEE Trans. Power Electron.*, vol. 28, no. 7, pp. 3614–3626, Jul. 2013.

[4] J. M. Rivas, Y. Han, O. Leitermann, A. D. Sagneri, and D. J. Perreault, "A high-frequency resonant inverter topology with low-voltage stress," *IEEE Trans. Power Electron.*, vol. 23, no. 4, pp. 1759–1771, Jul. 2008.

[5] J. M. Rivas, O. Leitermann, Y. Han, and D. J. Perreault, "A very high frequency DC–DC converter based on a class ϕ_2 resonant inverter," *IEEE Trans. Power Electron.*, vol. 26, no. 10, pp. 2980–2992, Oct. 2011.

[6] S. V. Cheong, H. Chung, and A. Ioinovici, "Inductorless DC-to-DC converter with high power density," *IEEE Trans. Ind. Electron.*, vol. 41, no. 2, pp. 208–215, Apr. 1994.

[7] O.-C. Mak, Y.-C. Wong, and A. Ioinovici, "Step-up DC power supply based on a switched-capacitor circuit," *IEEE Trans. Ind. Electron.*, vol. 42, no. 1, pp. 90–97, Feb. 1995.

[8] B. Wu, S. Li, K. Ma Smedley, and S. Singer, "A family of two-switch boosting switched-capacitor converters," *IEEE Trans. Power Electron.*, vol. 30, no. 10, pp. 5413–5424, Oct. 2015.

[9] B. Wu, S. Li, Y. Liu, and K. M. Smedley, "A new hybrid boosting converter for renewable energy applications," *IEEE Trans. Power Electron.*, vol. 31, no. 2, pp. 1203–1215, Feb. 2016.

[10] S. C. O. Mathuna, T. O'Donnell, N. Wang, and K. Rinne, "Magnetics on silicon: An enabling technology for power supply on chip," *IEEE Trans. Power Electron.*, vol. 20, no. 3, pp. 585–592, May 2005.

[11] M. Gerber, J. A. Ferreira, N. Seliger, and I. W. Hofsajer, "Integral 3-D thermal, electrical and mechanical design of an automotive DC/DC converter," *IEEE Trans. Power Electron.*, vol. 20, no. 3, pp. 566–575, May 2005.

[12] X. Liu, X. Jing, and G.-Q. Lu, "Chip-scale packaging of power devices and its application in integrated power electronics modules," *IEEE Trans. Adv. Packag.*, vol. 24, no. 2, pp. 206–215, May 2001.

[13] S. Ji, D. Reusch, and F. C. Lee, "High-frequency high power density 3-D integrated gallium-nitride-based point of load module design," *IEEE Trans. Power Electron.*, vol. 28, no. 9, pp. 4216–4226, Sep. 2013.

[14] F. C. Lee and Q. Li, "High-frequency integrated point-of-load converters: Overview," *IEEE Trans. Power Electron.*, vol. 28, no. 9, pp. 4127–4136, Sep. 2013.

[15] S. C. O. Mathuna *et al.*, "Packaging and integration technologies for future high-frequency power supplies," *IEEE Trans. Ind. Electron.*, vol. 51, no. 6, pp. 1305–1312, Dec. 2004.

[16] M. Gerber, J. A. Ferreira, I. W. Hofsajer, and N. Seliger, "High density packaging of the passive components in an automotive DC/DC converter," *IEEE Trans. Power Electron.*, vol. 20, no. 2, pp. 268–275, Mar. 2005.

[17] J. Popovic and J. A. Ferreira, "Converter concepts to increase the integration level," *IEEE Trans. Power Electron.*, vol. 20, no. 3, pp. 558–565, May 2005.

[18] A. L. Gattozzi, S. P. Pish, and J. A. Pappas, "Effect of converter packaging techniques on device electrical conduction," *IEEE Trans. Magn.*, vol. 39, no. 1, pp. 418–421, Jan. 2003.

[19] S. Sugahara, K. Yamada, M. Edo, T. Sato, and K. Yamasawa, "90% high efficiency and 100-W/cm^3 high power density integrated DC–DC converter for cellular phones," *IEEE Trans. Power Electron.*, vol. 28, no. 4, pp. 1994–2004, Apr. 2013.

[20] W. A. Roshen, R. L. Steigerwald, R. J. Charles, W. G. Earls, G. S. Claydon, and C. F. Saj, "High-efficiency, high-density MHz magnetic components for low profile converters," *IEEE Trans. Ind. Appl.*, vol. 31, no. 4, pp. 869–878, Jul./Aug. 1995.

[21] W. Zhang, Y. Su, M. Mu, D. J. Gilham, L. Qiang, and F. C. Lee, "High-density integration of high-frequency high-current point-of-load (POL) modules with planar inductors," *IEEE Trans. Power Electron.*, vol. 30, no. 3, pp. 1421–1431, Mar. 2015.

[22] E. Waffenschmidt, B. Ackermann, and J. A. Ferreira, "Design method and material technologies for passives in printed circuit board embedded circuits," *IEEE Trans. Power Electron.*, vol. 20, no. 3, pp. 576–584, May 2005.

[23] M. H. Lim, J. D. van Wyk, and F. C. Lee, "Hybrid integration of a low voltage, high-current power supply buck converter with an LTCC substrate inductor," *IEEE Trans. Power Electron.*, vol. 25, no. 9, pp. 2287–2298, Sep. 2010.

[24] Q. Li, Y. Dong, F. C. Lee, and D. Gilham, "High-density low-profile coupled inductor design for integrated point-of-load converters," *IEEE Trans. Power Electron.*, vol. 28, no. 1, pp. 547–554, Jan. 2013.

[25] L. Wang, Y. Pei, X. Yang, and Z. Wang, "Design of ultrathin LTCC coupled inductors for compact DC/DC converters," *IEEE Trans. Power Electron.*, vol. 26, no. 9, pp. 2528–2541, Sep. 2011.

[26] M. Mino, T. Yachi, A. Tago, K. Yanagisawa, and K. Sakakibara, "A new planar microtransformer for use in micro-switching converters," *IEEE Trans. Magn.*, vol. 28, no. 4, pp. 1969–1973, Jul. 1992.

[27] E.-J. Yun, M. Jung, C. I. Cheon, and H. G. Nam, "Microfabrication and characteristics of low-power high-performance magnetic thin-film transformers," *IEEE Trans. Magn.*, vol. 40, no. 1, pp. 65–70, Jan. 2004.

[28] I. Kowase, T. Sato, K. Yamasawa, and Y. Miura, "A planar inductor using Mn-Zn ferrite/polyimide composite thick film for low-voltage and large-current DC-DC converter," *IEEE Trans. Magn.*, vol. 41, no. 10, pp. 3991–3993, Oct. 2005.

[29] L. Wang, Y. Pei, X. Yang, Y. Qin, and Z. Wang, "Improving light and intermediate load efficiencies of buck converters with planar nonlinear inductors and variable on time control," *IEEE Trans. Power Electron.*, vol. 27, no. 1, pp. 342–353, Jan. 2012.

[30] M. H. F. Lim, J. D. van Wyk, and Z. Liang, "Internal geometry variation of LTCC inductors to improve light-load efficiency of DC-DC converters," *IEEE Trans. Compon. Packag. Technol.*, vol. 32, no. 1, pp. 3–11, Mar. 2009.

[31] M. H. Lim, J. D. van Wyk, F. C. Lee, and K. D. T. Ngo, "A class of ceramic-based chip inductors for hybrid integration in power supplies," *IEEE Trans. Power Electron.*, vol. 23, no. 3, pp. 1556–1564, May 2008.

[32] R. Hahn, S. Krumbholz, and H. Reichl, "Low profile power inductors based on ferromagnetic LTCC technology," in *Proc. 56th Electron. Compon. Technol. Conf.*, 2006, pp. 528–533.

[33] M. Mu, Y. Su, Q. Li, and F. C. Lee, "Magnetic characterization of low temperature co-fired ceramic (LTCC) ferrite materials for high frequency power converters," in *Proc. 2011 IEEE Energy Convers. Congr. Expo.*, Sep. 17–22, 2011, pp. 2133–2138.

[34] Y. Su, Q. Li, M. Mu, D. Gilham, D. Reusch, and F. C. Lee, "Low profile LTCC inductor substrate for multi-MHz integrated POL converter," in *Proc. 2012 27th Annu. IEEE Appl. Power Electron. Conf. Expo.*, Feb. 5–9, 2012, pp. 1331–1337.

[35] Q. Li and F. C. Lee, "High inductance density low-profile inductor structure for integrated point-of-load converter," in *Proc. 2009 24th Annu. IEEE Appl. Power Electron. Conf. Expo.*, Feb. 15–19, 2009, pp. 1011–1017.

[36] Y. Su, Q. Li, and F. C. Lee, "Design and evaluation of a high-frequency LTCC inductor substrate for a three-dimensional integrated DC/DC converter," *IEEE Trans. Power Electron.*, vol. 28, no. 9, pp. 4354–4364, Sep. 2013.

[37] M. Chen, M. Araghchini, K. K. Afridi, J. H. Lang, C. R. Sullivan, and D. J. Perreault, "A systematic approach to modeling impedances and current distribution in planar magnetics," *IEEE Trans. Power Electron.*, vol. 31, no. 1, pp. 560–580, Jan. 2016.

[38] J. M. Lopera, M. J. Prieto, A. M. Pernia, and F. Nuno, "A multi-winding modeling method for high frequency transformers and inductors," *IEEE Trans. Power Electron.*, vol. 18, no. 3, pp. 896–906, May 2003.

[39] J. Qiu and C. R. Sullivan, "Design and fabrication of VHF tapped power inductors using nanogranular magnetic films," *IEEE Trans. Power Electron.*, vol. 27, no. 12, pp. 4965–4975, Dec. 2012.

[40] J. Lu, H. Jia, X. Wang, K. Padmanabhan, W. G. Hurley, and Z. J. Shen, "Modeling, design, and characterization of multiturn bondwire inductors with ferrite epoxy glob cores for power supply system-on-chip or system-in-package applications," *IEEE Trans. Power Electron.*, vol. 25, no. 8, pp. 2010–2017, Aug. 2010.

Laili Wang (S'07–M'13–SM'15) received the B.S., M.S. and Ph.D. degrees in electrical engineering from Xi'an Jiaotong University, Xi'an, China, in 2004, 2007 and 2011, respectively.

In 2011, he became a Postdoctoral Fellow with the Electrical Engineering Department, Queen's University, Kingston, ON, Canada. In 2013, he started to work as a Research Fellow in Queen's University. Since 2014, he has been with the Research Center, Sumida Inc., Canada. In 2016, he joined Xi.an Jiaotong University. He is currently a Professor with the Department of Electrical and Computer Engineering. His research interests include package and integration, wireless charging, and energy harvesting.

Wenbo Liu (S'16) received the B.S. degree in electrical engineering and automation from Zhejiang University, Hangzhou, China, in 2014, and is currently working toward the Ph.D. degree in power electronics at Queen's University, Kingston, ON, Canada.

His current research interests include high power density point-of-load converters, design and optimization of magnetic components, thermal modeling and finite-element method simulation and analysis.

Doug Malcom received the B. Eng degree in electrical engineering from Lakehead University, Thunder Bay, ON, Canada, in 1982.

He was an Engineer and later Manager of the Magnetics group in Nortel (BNR) from 1982 to 1997, the Director of Pulse Canada from 1997 to 2001, the Director of the Sumida Magnetics Design Center, Ottawa, Canada, from 2002 to 2005, the President of Sumida America Components from 2005 to 2010, and currently the President of Sumida Technologies, Inc., Kingston, ON, Canada, and Sr. VP Global Common R&D of SUMIDA CORPORATION since 2010. His current interest is in growing the Power Supply in Inductor (PSI^2) product line.

Yan-Fei Liu (M'94–SM'97–F'13) received the Bachelor's and Master's degrees from the Department of Electrical Engineering, Zhejiang University, Hangzhou, China, in 1984 and 1987, respectively, and the Ph.D. degree from the Department of Electrical and Computer Engineering, Queen's University, Kingston, ON, Canada, in 1994.

He was a Technical Advisor with the Advanced Power System Division, Nortel Networks, Ottawa, Canada, from 1994 to 1999. Since 1999, he has been with Queen's University, where he is currently a Professor with the Department of Electrical and Computer Engineering. He has authored more than 200 technical papers in the IEEE transactions and conferences, and holds 20 U.S. patents. His current research interests include digital control technologies for high-efficiency, fast dynamic response dc–dc switching converter and ac–dc converter with power factor correction, resonant converters and server power supplies, and LED drivers.

Dr. Liu is a Principal Contributor for two IEEE standards. He is the Vice President of Technical Operations of IEEE Power Electronics Society (PELS) from 2017 to 2018. He has been an Editor for IEEE JOURNAL OF EMERGING AND SELECTED TOPICS OF POWER ELECTRONICS (JESTPE) since 2013. He will be the General Chair of IEEE Energy Conversion Congress and Exposition (ECCE) to be held in Baltimore, USA, in 2019. His major service to IEEE are listed as follows: a Guest Editor-in-Chief for the special issue of Power Supply on Chip of IEEE TRANSACTIONS ON POWER ELECTRONICS from 2011 to 2013; a Guest Editor for special issues of JESTPE: Miniaturization of Power Electronics Systems in 2014 and Green Power Supplies in 2016; as the Co-General Chair of ECCE held in Montreal, Canada, in September 2015; the Chair of PELS Technical Committee (TC1) on Control and Modeling Core Technologies from 2013 to 2016; since 2013; Chair of PELS Technical Committee (TC2) on Power Conversion Systems and Components from 2009 to 2012. He was a recipient of the Premier's Research Excellence Award in 2000 in Ontario, Canada. He was also a recipient of the Award of Excellence in Technology in Nortel in 1997.